Cascaded four-wave mixing generation with pumping in the normal dispersion regime

Ying Li (李 荧), Jing Hou (侯 静)*, Zongfu Jiang (姜宗福), and Liangjin Huang (黄良金)

College of Optoelectronic Science and Engineering, National University of Defense Technology, Changsha 410073, China

**Corresponding author: houjing25@sina.com*

Received August 23, 2013; accepted January 15, 2014; posted online February 28, 2014

we report on the generation of cascaded four-wave mixing (CFWM) in a photonic crystal fiber with a high peak power picosecond pulse pumping in the normal dispersion region and a weak continuous wave seeded. We also experimentally investigate the dependence of CFWM bandwidth on the seeding wavelengths. Experimental results demonstrate the existence of optimum seeding wavelengths for broadband CFWM even though the pulse wavelength is 50 nm shorter than the zero dispersion wavelength. And CFWM products spanning more than 300 nm are experimentally obtained.

OCIS codes: 190.4370, 190.4380.

doi: 10.3788/COL201412.031901.

Frequency comb[1,2] has drawn much attention because its potential applications in many research fields such as wavelength division multiplexing system[3], chemical sensing[4], astrophysical spectrometer calibration and metrology[5]. In certain applications, cascaded four-wave mixing (CFWM) is exploited to achieve broadband frequency comb[3,5]. As a result, a number of previous reviews of CFWM generation have been written[6−8], and CFWM products centered on 1.5 μm have been numerically and experimentally obtained[9−12]. In the experiments, pump signals were mostly pumped in the anomalous dispersion regimes of the highly nonlinear fibers (HNLFs) or photonic crystal fibers (PCFs). That is because in the anomalous dispersion regime the gain band of modulation instability (MI, time-domain description of the same physic as FWM) is much broader than that of the normal dispersion region[13]. In addition, cascaded MI is much easier to be generated when a single signal is pumped into a short segment of fiber[14]. Recently, CFWM products centered on 1.0 μm have also been experimentally[15] realized using a PCF with two zero dispersion wavelengths (ZDWs). And this year, we obtained CFWM with arbitrary frequency pitch centered on 1.0 μm by pumping in the anomalous dispersion region[14]. For the scheme we proposed in that work, a high-power pulse pump and a weak continuous wave (CW) seed are injected into a short segment of PCF, FWM occur between them and the first-order idlers will be generated on both sides of the pulse pump and the CW seed. Furthermore, FWM processes followed occur involving the first-order idlers generated previously, creating second-order and even higher-order idlers with new frequencies. Through this cascaded process, many spectral peaks will be obtained at the output end of PCF. Different from the previous studies, we pump the high power pulse in the normal dispersion region of the PCF, which has the ZDW of 50 nm shorter than the pump central wavelength, in which case no cascaded MI can be observed when only pulse pumping. Dependence of the CFWM bandwidth on the seeding wavelengths is particularly investigated.

The experimental setup is shown in Fig.1. In the experiments a picosecond pulse signal and a CW signal are used. The pulse signal comes from a Nd:YAG Q-switched microchip laser (NP-10820, Teem Photonics, France), running at 1064 nm and emitting of 0.6 ns (FWHM) pulses with 15-kW peak power at a 7.3-kHz repetition rate. For CW signal generator, a 300-mW laser diode (LD) centered at 976-nm provides the pump. The fiber ring cavity consists of a WDM, a 60-cm Yb-doped fiber (YDF, Liekie Yb-1200-4/125, nlight, USA), a tunable band pass filter (BPF) manufactured by Agiltron Inc., an isolator (ISO), and a coupler. Wavelength tuning from 1010 to 1097 nm is achieved by the tunable BPF. As displayed in Fig. 1, two signals are coupled with a WDM and launched into PCF. The reflective port of the WDM in Fig. 1 is connected with the output end of CW signal. And this port has a very low reflectance near the wavelength of 1064 nm. So the CW signal at 1060−1069 nm cannot be successfully coupled into PCF. The PCF we use in the experiments has a core diameter of 7.3 μm, hole-to-hole spacing Λ around 5.42 μm, air hole diameter $d = 3.54$ μm, effective mode field area (MFA, $A_{\rm eff}$) $A_{\rm eff} = 26$ μm^2. Its calculated dispersion profile and group velocity from a fully vectorial finite element mode solver (Comsol Multiphysics) are displayed in Fig. 2. Its ZDW locates at 1117 nm. So the 1064-nm pulse pumps in the normal dispersion region. Spectra after the PCF are monitored with an optical spectrum analyzer (OSA) operating in the range of 600−1700 nm.

Firstly, we investigate the parametric gain in this PCF. If the pump waves are assumed to remain undepleted during the FWM process, parametric gain g is given by[13,16]

$$g = \sqrt{(\gamma P_0)^2 - (\kappa/2)^2}, \tag{1}$$

where γ is the nonlinear parameter, P_0 is the pump power, the phase mismatch term κ is given by $\kappa = 2\gamma P_0 + 2\sum_{m=1}^{\infty}[\beta_{2m}/(2m)]\Omega^{2m}$, Ω is the angular frequency

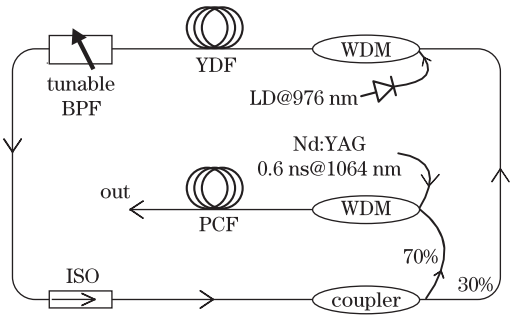

Fig. 1. Schematic of the whole experiment.

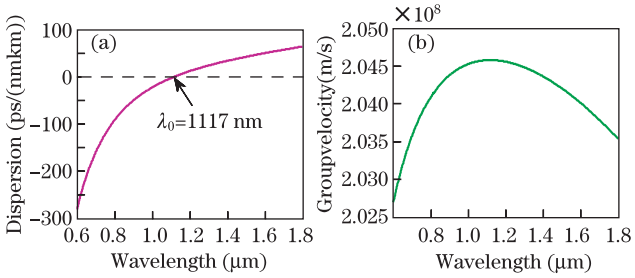

Fig. 2. (Color online) (a) Calculated dispersion profile and (b) group velocity of the PCF used in the experiments.

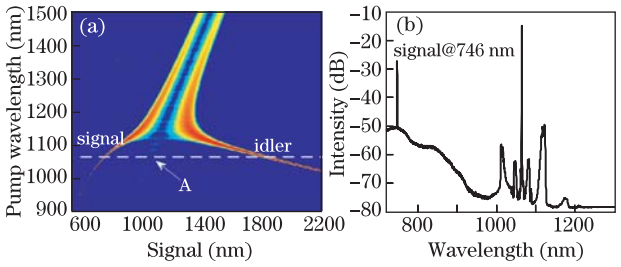

Fig. 3. (Color online) (a) Parametric gain for different pump wavelengths. (b) Measured spectrum when only pulse is pumped.

shift from the pump, and β_{2m} represent the different even-order dispersion coefficients at the pump wavelength. Figure 3(a) displays the parametric gain as the function of wavelengths. Pump central wavelength ranges from 900 to 1500 nm. Input peak power is selected as 5 kW. Notably, parametric gain bands in the normal and anomalous dispersion regions are qualitative differences in the gain spectra. We see that the gain spectrum for the anomalous dispersion regime pumping at 1160 nm consists of a relatively broad gain band (∼150 nm). The horizontal dashed line indicates the pump wavelength at 1064 nm, where gain bands consist of narrow-band peaks displaced from the pump wavelengths. In the experiments we get the same result. As displayed in Fig. 3(b), signal wave at about 746 nm is generated by phase-matched FWM. While the idler wave is excess the detection limit of OSA. Besides the Stokes and anti-Stokes wave generated by stimulated Raman scattering (SRS), there are another two generated peaks very close to the pump wavelength in Fig. 3(b). And their wavelengths coincide with that of gain bands marked by the arrow in Fig. 3(a). In the following discussion we will find the small gains play an important role for the generation of broad band CFWM.

As described in Ref. [14], SRS plays a critical role in the spectral broadening when pumping long pulse in the normal dispersion region. So cascaded SRS or CFWM will be obtained if we seed the CW signal at the first order Stokes wave. However, the CFWM with seeding at 1034 nm has not been successfully generated. In the following experiments, we investigate the CFWM generation with seeding at different wavelengths in this PCF comprehensively.

Using the cut-back method, we find the optimum fiber length is about 0.9 m when 25 mW of pulse pump power can be launched into it. Average power of CW seed is selected as ∼25 mW, which is 2×10^5 times weaker than the pulse peak power. In Fig. 4, solid lines summarize the experimental results for seeding the CW on the Stokes side (Fig. 4(b)) as well as the anti-Stokes (Fig. 4(a)) side of the pulse. Different colors indicate the CFWM products with different seeding wavelengths. For comparison purposes, we also include, in Fig. 4, the spectra for only pulse pumping (dashed lines). Obviously, the first Stokes wave of SRS is found to exhibit double-peak structure corresponding to peaks at about 1117 and 1123 nm. With the help of FWM, the first anti-Stokes wave of SRS is also clearly observed. This will be conducive to the generation of CFWM.

As seen clearly in Fig. 4, bandwidth of the CFWM has a remarkable dependence on CW wavelengths, regardless of seeding on the Stokes side or the anti-Stokes side. CFWM products are not efficiently generated with seeding much close to the pulse pump is also not the suggested way of producing broadband CFWM, like the cases of seeding at 1054 or 1075 nm. Although, seeding close to pulse will make the phase or group-velocity mismatching much smaller. Peaks nearby are indeed generated through FWM. However, the generated peaks are cross the maximum of Raman gain. Without the help of SRS, CFWM cannot be efficiently produced because of pumping in the normal dispersion region. Even when we seed the CW at the first anti-Stokes wave (1016 nm), broadband CFWM products can neither be generated. This is due to the inefficiency of power transfer from CW to the first Stokes peak through FWM. So that cascaded SRS are not efficiently generated. And the CFWM generation is also been influenced. Compared the spectra with each other, we find that there are two optimum seeding wavelengths for broadband CFWM: one is on the Stokes side and the other is on the anti-Stokes side.

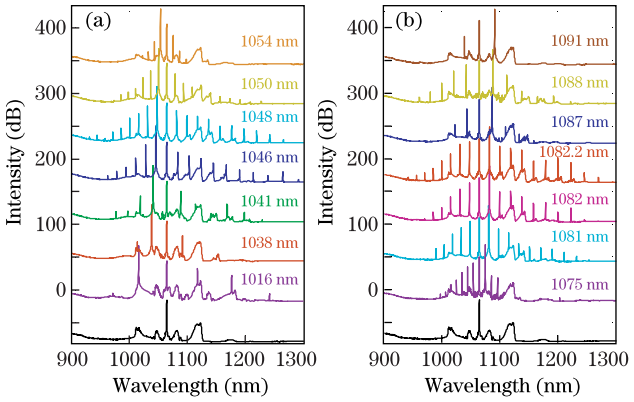

Fig. 4. (Color online) Measured spectra for only pulse pumping (dashed lines) and CW seeded (solid lines) at different wavelengths.

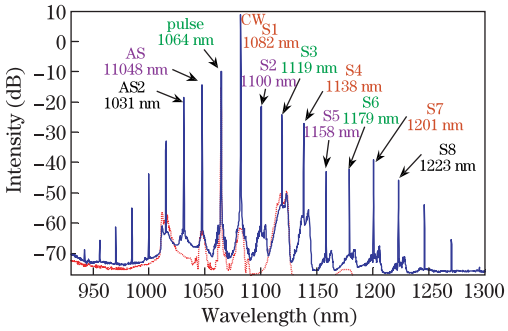

Fig. 5. (Color online) Measured spectrum for CW seeded at 1082 nm.

CFWM products in the two cases have something in common. That is the third peak away from the pulse central wavelength on the Stokes side just locates at the maximum of Raman gain (see the spectra with seeding at 1082 and 1048 nm). And the seeding wavelengths locate at the gain bands.

To get more insight into the CFWM generation with the help of SRS, we investigate the specific condition under which the CW wavelength is fixed at 1082 nm. Figure 5 shows a zoom of the spectrum for the cases with only pulse pumping (dotted red line) and CW signal seeded (solid blue line). Note that the spectral window of the CFWM has a width of larger than 300 nm at a level of -70 dB. 19 peaks of the CFWM products can be identified clearly, having an optical signal-to-noise ratio (OSNR) higher than 3 dB. There are several notable features in Fig. 5. In the basement, more than two double-peak structures can be observed, especially on the Stokes side. And the peaks on the Stokes side are much more than that of the anti-Stokes side. Based on these two features, we give an estimate that SRS plays a critical role in the CFWM generation. As marked in Fig. 5, CW signal at 1082 nm is regarded as the first order on the Stokes side (marked as S1), and peak at 1048 nm is regarded as the first order on the anti-Stokes side (marked as AS1). According to the numerical calculations, the first two order Stokes waves of 1048 nm locate at 1100 and 1158 nm, which coincide with the peaks of S2 and S5 in Fig. 5. The first two order Stokes lines of 1082 nm locate at 1138 and 1201 nm, which coincide with the peaks of S4 and S7. So the CFWM generation can be explained as follows. With 1082 nm locating at the peak of the parametric gain band (indicated by arrow in Fig. 3(a)), peaks close to the pump such as AS1 and S2 are firstly generated when the pulse at 1064 nm and CW at 1082 nm are launched into PCF. And then, S2 extracts a portion of power from AS1 with the help of SRS. So we observed the double-peak structure in the basement. Meanwhile, there is a sharp peak at 1100 nm generated by FWM, which also serves as a probe beam. And it can be further amplified because of the Raman gain. Similarly, peak of 1119 nm extracts power from the pulse pump through SRS, until it becomes strong enough to seed the generation of the next Stokes line at 1179 nm. Peaks of S4 and S7 get the power from S1. And then more peaks in the anti-Stokes side are generated through FWM with the trigger of peaks in the Stokes side. Higher the order of the peak is, farther it is away from the ZDW, larger the phase or group-velocity mismatching is, and harder it is for FWM to be generated. As a result, peaks on the anti-Stokes side are much less than that on the Stokes side.

In conclusion, we demonstrate a mechanism to generate broadband CFWM centered on 1.0 μm with pulse pumping in the normal dispersion region. Dependence of CFWM bandwidth on the CW seeding wavelengths is experimentally researched. And we find the optimum seeding wavelengths for the efficient generation of CFWM. The underlying physical mechanisms are also investigated. With the combined effort of SRS and FWM, CFWM products with the bandwidth of more than 300 nm are experimentally obtained.

This work was supported by the National Natural Science Foundation of China under Grant No. 61235008.

References

1. S. A. Diddams, J. Opt. Soc. Am. B **27,** B51 (2010).
2. Y. Dou, H. Zhang, Y. Wang, and M. Yao, Chin. Opt. Lett. **11,** 070603 (2013).
3. A. E. H. Oehler, S. C. Zeller, K. J. Weingarten, and U. Keller, Opt. Lett. **33,** 2158 (2008).
4. A. Schliesser, M. Brehm, F. Keilmann, and D. van der Weide, Opt. Express **13,** 9029 (2005).
5. F. C. Cruz, Opt. Express **16,** 13267 (2008).
6. N. S. Shahabuddin, Z. Yusoff, H. Ahmad, and S. W. Harun, Chin. Opt. Lett. **9,** 061407 (2011).
7. C. S. Arismar Jr., J. M. C. Boggio, H. E. Hernandez-Figueroa, H. L. Fragnito, and J. C. Knight, in *Proceedings of 33rd Eurpopean Conference and Ehxibition on Optical Communication (ECOC)* 1 (2007).
8. X. Xiao, in *Proceedings of Asia Communications and Photonics Conference* AF4A.68 (2012).
9. Arismar Cerqueira S. Jr., J. M. Chavez Boggio, A. A. Rieznik, H. E. Hernandez-Figueroa, H. L. Fragnito, and J. C. Knight, Opt. Express **16,** 2816 (2008).
10. Cerqueira Arismar Jr. S., J. D. Marconi, H. E. Hernandez-Figueroa, and H. L. Fragnito, Opt. Commun. **282,** 4436 (2009).
11. P. Zuo, T. Fuji, and T. Suzuki, Opt. Express **18,** 16183 (2010).
12. N. A. Cholan, M. H. Al-Mansoori, A. S. M. Noor, A. Ismail, and M. A. Mahdi, Opt. Express **21,** 6131 (2013).
13. J. M. Dudley, G. Genty, and S. Coen, Rev. Mod. Phys. **78,** 1135 (2006).
14. J. Hou, Y. Li, J. Leng, P. Zhou, and Z. Jiang, Appl. Phys. B **113,** 611 (2013).
15. H. Sayinc, M. Wysmolek, J. M. Chavez Boggio, R. Haynes, M. M. Roth, U. Morgner, J. Neumann, and D. Kracht, Appl. Phys. B **110,** 299 (2013).
16. G. P. Agrawal, *Nonlinear Fiber Optics* (4th ed.) (Academic Press, 2006).